AIAA 2002-2468

Slat Cove Noise Modeling: *A Posteriori* Analysis of Unsteady RANS Simulations

M. Choudhari, M. Khorrami, D. Lockard, and H. Atkins
NASA Langley Research Center
Hampton, VA

G. Lilley
Penn State University
State College, PA

8th AIAA/CEAS Aeroacoustics Conference & Exhibit
17-19 June 2002
Breckenridge, CO

**For permission to copy or to republish, contact the copyright owner named on the first page.
For AIAA-held copyright, write to AIAA Permissions Department,
1801 Alexander Bell Drive, Suite 500, Reston, VA, 20191-4344.**

SLAT COVE NOISE MODELING: *A POSTERIORI* ANALYSIS OF UNSTEADY RANS SIMULATIONS

Meelan Choudhari[†], Mehdi R. Khorrami[*], David P. Lockard[†], Harold L. Atkins[†]
M.S. 128, NASA Langley Research Center, Hampton, VA 23681
and
Geoffrey M. Lilley[**]
Pennsylvania State University, University Park, PA 16802.

Abstract

A companion paper by Khorrami et al[1] demonstrates the feasibility of simulating the (nominally) self-sustained, large-scale unsteadiness within the leading-edge slat-cove region of multi-element airfoils using unsteady Reynolds-Averaged Navier-Stokes (URANS) equations, provided that the turbulence production term in the underlying two-equation turbulence model is switched off within the cove region. In conjunction with a FfowcsWilliams-Hawkings solver, the URANS computations in ref. [1] were shown to capture the dominant portion of the acoustic spectrum attributed to slat noise, as well as reproducing the increased intensity of slat cove motions (and, correspondingly, far-field noise as well) at the lower angles of attack. This paper examines that simulation database, augmented by additional simulations, with the objective of transitioning this apparent success to aeroacoustic predictions in an engineering context. As a first step towards this goal, the simulated flow and acoustic fields are compared with experiments[2-5] and simplified analytical models[6,7]. Rather intense near-field fluctuations in the simulated flow are found to be associated with unsteady separation along the slat bottom surface, relatively close to the slat cusp. Accuracy of the laminar-cove simulations in this near-wall region is raised to be an open issue. The adjoint Green's function approach is also explored in an attempt to identify the most efficient noise source locations.

1. Introduction

In studies on airframe noise, it is found that a primary source of noise generation on high-lift devices involves an interaction between large-scale energy-containing flow structures and the solid surfaces. This is especially true near a flap side edge or within the slat cove of a multi-element airfoil configuration as indicated by the favorable comparison between computational predictions based on the large-structure paradigm[1,8-9] and the experimental measurements, either at the surface,[10] or in the far field[10-12]. Accordingly, the established approach in modern investigations[13] of airframe noise has been, first, to identify and model the unsteady disturbances supported by relevant elements of the flow field and, then, to propagate this information to the far field via some form of acoustic analogy. The part related to far-field propagation is conceptually straightforward, although its numerical implementation might require some thought and ingenuity as described in refs. [14]-[16]. Consequently, characterization of the unsteady flow structures has become the crux of modeling the large class of airframe noise sources associated with separated/free-shear flows.

The required characterization of unsteady disturbances may be attempted at various levels of the modeling hierarchy, depending on the type of noise source involved and the specific purpose behind the investigation and the level of accuracy desired. For instance, the large-scale unsteadiness in a flap-side-edge

---

[†] Aerospace Technologist, Computational Modeling and Simulation Branch, Senior Member AIAA
[*] Aerospace Technologist, Computational Modeling and Simulation Branch, Associate Fellow AIAA
[**] Visiting Research Professor, Fellow AIAA

Copyright © 2002 by the American Institute of Aeronautics and Astronautics, Inc. No copyright is asserted in the United States under Title 17, U.S. Code. The U.S. Government has a royalty-free license to exercise all rights under the copyright claimed herein for Governmental Purposes. All other rights are reserved by the copyright owner.

many of the acoustically relevant fluid dynamical processes within the slat-cove flow. It serves as a visual reference during much of the discussion presented in this section. For an expanded description of the various flow phenomena observed during the simulations, as well as details of the high-lift configuration, computational grid and flow solver, and the zonal modeling concept employed, the reader is referred to refs. [1, 21-23].

2.1 Mean flow characteristics and turbulent kinetic energy (TKE) distributions

In recent work related to semi-empirical prediction of jet-noise[24, 25], turbulence field data based on steady RANS computations has been used as an approximate means to characterize the local amplitude (and, possibly, length/time scale) of turbulence in a spatially inhomogeneous flow. Extending this concept to airframe noise predictions in a design environment may be feasible and, certainly, useful. This section presents a comparison of the mean flow field and turbulent kinetic energy distribution as computed with steady RANS, URANS with the zonal model incorporating zero turbulence production within the slat cove, and the experiments by Takeda et al[2] for a similar cove flow on a high-lift configuration. Both computations utilize Menter's k-omega SST model.[20]

2.1.1 8-deg AOA

We begin by comparing the time average of the computed unsteady flow with the corresponding steady RANS calculation for the case of 8 degree AOA. As indicated in Figs. 2a and 2b, a relatively close correspondence is observed between the two flow fields, with both solutions indicating (i) the development of a mean shear layer as the flow separates from the cusp (ii) the flow impingement somewhat upstream of the slat trailing edge; and (iii) the recirculating flow along the slat pressure surface. These features are also consistent, in a qualitative sense, with the experimental measurements[2] based on Particle Image Velocimetry (PIV).

Some quantitative differences are, however, apparent between the two computed solutions. Specifically, the strength of the recirculating flow in the unsteady RANS solution is relatively stronger, primarily as a result of the strong vortex structures advected along the slat pressure surface. Recall from Fig.1 that these vortices originate primarily from the cusp shear layer, but remain trapped within the cove region for long durations. As described by KSL, the convective feedback associated with these vortices also leads to a quicker roll-up of the shear layer (as compared to mixing layers without any feedback), which explains the higher rate of shear-layer growth in the unsteady case. The mean reattachment location is seen to compare rather well between the steady and unsteady computations.

Next, we compare the corresponding distributions of TKE. In the steady RANS case, the turbulence energy is a field variable for the two-equation turbulence model[20], whereas in the unsteady case it is obtained by averaging over instantaneous snapshots derived from the computations. Although the duration of the unsteady calculation was longer than twenty convection time units, evidence of mild statistical non-stationarity was noted in the case of 8 degrees AOA. The average shown in Fig. 2a corresponds to the entire data acquired after the initial transients had subsided.

In the unsteady case (Fig. 3a), higher TKE magnitudes along the slat pressure surface clearly reveal the signature of the convective feedback to the slat-cusp region via the recirculating flow. On the other hand, the steady RANS calculation cannot fully anticipate the dynamical significance of this feedback, as seen from a comparison between Figs. 3a and 3b. According to steady RANS, the peak TKE levels occur in the immediate vicinity of the reattachment location (Fig. 3b). In contrast, the unsteady solution indicates an increased TKE both near the mean reattachment and along the feedback loop.

The peak magnitudes of TKE in the cove region are also higher in the steady case. The two-equation turbulence model in that case is designed to capture the kinetic energy associated with all unsteady scales of motion. In the URANS solution with a pseudo-laminar slat cove region, there is no obvious mechanism to capture the contributions due to either the spanwise scales of motion or any intermediate- through small-scale disturbances that are left unresolved by the combination of numerical scheme and computational grid used. A comparison between Figs. 3a and 3b suggests that the unresolved scales in the unsteady case may account for a significant fraction of the overall fluctuating kinetic energy.

The turbulent kinetic energy (TKE) distribution measured by Takeda et al. [2] at 5 degree AOA is reproduced in Fig. 3c. The measured TKE distribution at 10 degrees AOA is similar to the 5 degree case, except that the overall TKE levels are lower by about 15 percent. Clearly, the measured TKE data share the same features as found in the computations: namely, higher TKE levels both within the shear layer and in the vicinity of the reattachment location. The measured data also indicates the elevated TKE levels in the re-circulating flow along the slat pressure surface, in agreement with the unsteady computations. However, the measured fluctuation levels near the cusp are weaker than those in the reattachment region, which is unlike the unsteady result shown in Fig. 3a. The experiment is also seen to

2.2.3 Surface pressure fluctuations

It is not uncommon to use pressure fluctuation data at the solid surface (as predicted with a suitable model for nearfield unsteadiness) towards predictions of far-field acoustics[7]. To gain some insight into the spatio-temporal structure of surface pressure fluctuations caused by the disorderly motion of computed slat-cove vortices, a plot of simulteneous pressure histories along the slat pressure surface is presented in Fig. 6. The data used represent a subset of the complete simulation for the 4 deg case. The abscissa of the plot corresponds to distance measured along the slat pressure surface and the locations of the trailing edge and slat cusp are also indicated in the figure. Consistent with the hot spots in the TKE distributions examined earlier, relatively intense pressure fluctuations are observed near s/L = 0.09, i.e., in the region where the recirculating flow (or wall jet) separates from the surface. Also worth noting are a pair of secondary "events" on each side of s/L ≈ 0.05, i.e. closer to the mean reattachment location of s/L ≈ 0.04.

An alternating pattern of positive and negative overpressures (corresponding to repeated ejection of vorticity from the recirculating wall jet) is evident near s/L=0.09. In the 4 degree case, the root-mean-square (r.m.s.) values of these fluctuation are significantly higher than those in the vicinity of the reattachment location. The above pattern is swept past the surface at phase velocities that appear to fall within a narrow range. To quantify the "average" phase velocity, as well as to understand how pressure fluctuations at any given location along the surface correlate with pressure histories at the adjacent locations, space-time correlation maps for surface pressure fluctuations were computed. Figure 7a shows one such map, with the reference probe being close to the location of peak pressure fluctuation along the surface, i.e., near the point of secondary separation. The plot suggests fairly localized covariance distribution, both in space and time, with a phase velocity of approximately 0.6 times the free-stream speed.

Figure 7b shows a similar plot corresponding to a reference probe location near s/L ≈ 0.075. The autocorrelation function for the fluctuating pressure at this location, which is given by a constant s/L cross-section of Fig. 7b, has a slowly decaying oscillatory behavior even for large values of the time lag t (which has been scaled with respect to speed of sound c and cruise chord L) . The period of these oscillations is comparable to the longer time scale of flow advection along the length of the slat. The physical significance of this finding is not immediately obvious, although it might be indicative of the feedback associated with repeated passages of any given vortex through the recirculation zone.

2.2.4 Intermittent ejection of vorticity through gap

The unsteady slat-cove flow at lower angles of attack displays yet another feature that is intrinsically suppressed in a statistical analysis, yet may have a bearing on the relative significance of scattering near the leading and trailing edges of the slat. It corresponds to the progressively stronger yet intermittent ejection of vortex structures from the recirculating region as the AOA is decreased. Specifically, vortices that escape the recirculating zone get convected past the trailing edge of the slat and may interact nonlinearly with the Strouhal shedding from the edge. Whether or not such infrequent interactions can lead to significant noise generation is best clarified through a time-domain acoustic calculation, which we have not yet attempted.

3. Acoustic predictions based on URANS + FWH equation

Having established that many of the flow characteristics found by KSL agree favorably with the available measurements, the next step involves making analogous comparisons between the far-field acoustic predictions and measurement. The study by KSL has already established that the intensification of coherent structures at lower angles of attack also translates into an increased far-field acoustic intensity. This comparison was limited to the spectral shape at a single observer location, mainly due to limitations of the acoustic measurements within the LTPT[3]. To gain further confidence into the validity of such computations (or, alternatively, to obtain additional insights into the complex broadband noise source associated with a slat), extending such comparisons to include the directivity pattern and parametric variation of the far-field noise, particularly in terms of velocity scaling laws, is essential. Preliminary findings towards this objective are presented in this section, along with a discussion of issues related to comparisons of absolute sound pressure levels between simulations and experiments.

3.1 Velocity Scaling Laws for Computed Noise

One of the objectives in the LTPT experiments was to determine velocity scaling laws for both slat and flap noise, especially at Reynolds numbers approaching those under flight conditions. The LTPT data has been shown to collapse reasonably well with a nominally V^5 law[3], although the low-frequency data may be closer to a V^4 law. The 5^{th} power law is also consistent with slat noise measurements in other facilities, both at NASA Langley Research Center[5] and in Europe[4].

To determine the velocity scaling laws for the computed noise based on URANS with the zonal model, additional simulations were carried out for M=0.1 and M=0.3,

the real flow are only located over a finite span, but the predictions have used a two-dimensional noise propagation model. A relatively simple analysis for a finite length, but fully correlated line source suggested, however, that the error due to this approximation is likely to be under 2.5dB for the LTPT experiment. A final source of discrepancy between computed and measured noise levels is that the latter includes contributions from other potential noise sources, such as edge/gap-induced scattering of boundary-layer turbulence over the slat suction surface, which is not modeled in the URANS simulations.

For the purpose of understanding the basic noise generation mechanisms and determining the effect of Mach number and angle of attack changes, the two-dimensional approach should be sufficient. However, absolute levels can not be predicted with any level of certainty until these issues are addressed. In making comparisons with experimental data, the influence of measurement error on the interpretation of results must also be considered. Microphone array technology has advanced significantly from its inception, but uncertainty about absolute levels, especially for low frequencies in hard-wall tunnels, still exists.

3.4 Comparison with analytical models for slat-cove noise

The slat-noise component in itself is a complex aeroacoustic problem that involves a combination of interdependent noise generation mechanisms in overlapping frequency bands. Not all of these mechanisms have received sufficient consideration, so developing physics-based predictions for slat-cove noise in an engineering context is a challenge. The recent attempt by Guo[7] represents a promising start in that direction. Guo modeled the cove unsteadiness via vortex shedding from the slat cusp and trailing edge in the form of discrete, multiple point vortices that interact with both each other and the underlying steady flow. This model generates similar unsteady vortex motions that were observed in the URANS simulations with the zonal model although, of course, it cannot include any unsteady features tied to near-wall physics. The predicted f^{-2} roll-off in the noise spectrum at higher frequencies roughly agrees with that predicted with the URANS simulations (Fig. 8a), although his $V^{2.5}$ scaling for noise indicates a somewhat slower increase with velocity than the simulations. The strongly peaked directivity patterns predicted by Guo's model also need further verification.

The peak noise frequencies at 8 degree AOA are consistent with the hydrodynamic instability of the free shear layer emanating from the cusp. The hydrodynamic stability models do not, however, explain the higher frequency fluctuations observed in both URANS simulations and the measured far-field noise. Moreover, at the lower angles of attack, the URANS simulations indicate the linear instabilities of the mixing-layer flow to be even less applicable.

4. Effects of scattering by solid surfaces

The near-field analysis outlined in Section 2 provides some clues into dominant sources of near-field fluctuations. Understanding the conversion of these fluctuations into acoustic energy is a challenging problem. The sensitivity of sound to source interactions combined with surface diffraction effects complicate modeling efforts. However, some insight can be gained by regarding the source mechanism and noise propagation as independent. From section 2, some potential noise sources have already been identified from the regions of high turbulent kinetic energy, although further calculations involving the actual source terms in Lighthill's acoustic analogy are necessary. Mathematically, the radiated noise corresponds to the convolution of the acoustic source (i.e., near-field unsteadiness in the form of double-divergence of the Lighthill stress tensor) and a Green's function that satisfies appropriate boundary conditions at the solid surfaces. The character of the acoustic Green's function determines the filtering characteristics related to the conversion of vortical disturbances to acoustic radiation. A series of linearized Euler calculations are conducted to determine the character of the Green's function. (Related calculations of this type were presented earlier by Manoha et al.[26]) The problem is further simplified by assuming that mean flow effects can be neglected. This is a good assumption over most of the flow field, but the shear layer in the cove is likely to have some influence that is not being modeled.

The quadrature-free version of the discontinuous Galerkin method[27] is used to perform the calculations with 22,500 triangles on a grid that extends several chords from the airfoil. Fifth-order polynomial representations are used within each triangle, and curved elements are employed for solid surfaces to improve the representation of the geometry. Cases were run on different grids which showed only minor variations in the results. One set of calculations involved specifying monopole and dipole sources near the cusp and reattachment points. Fig. 11a shows the instantaneous pressure contours for an 8 kHz monopole source near the cusp. The contours show the complexity of the interactions between the scattering bodies producing null regions even when there is a direct line of sight with the source. Edge scattering, especially from the trailing edge of the flap, is also evident. Figure 11b presents the near-field directivities for the same monopole source but at

7. Guo, Y.P., "A Discrete Vortex Model for Slat Noise Prediction," NASA Contractor Report No. CRAD-9402-TR-5170, Oct. 2000.
8. Khorrami, M.R. and Singer, B.A., "Stability Analysis for Noise-Source Modeling of a Part-Span Flap," AIAA J., vol. 37, No. 10, 1999, pp. 1206-1212.
9. Streett, C.L., "Numerical Simulation of Fluctuations Leading to Noise in a Flap-Edge Flowfield,"AIAA Paper 98-0628, 1998.
10. Meadows, K. R., Brooks, T. F., Humphreys, W. M., Hunter, W. H., and Gerhold, C. H., "Aeroacoustic Measurements of a Wing-Flap Configuration," AIAA Paper 97-1595, 1997.
11. Storms, B.L., Takahashi, T.T., and Ross, J.C., "Aerodynamic Influence of a Finite-Span Flap on a Simple Wing," SAE Paper 951977, Sept. 1995.
12. Streett, C.L., Lockard, D.P., and Singer, B.A, unpublished data, 1999.
13. Macaraeg, M. G., "Fundamental Investigations of Airframe Noise,". AIAA Paper 98-2224, 1998.
14. F. Farassat and Kenneth S. Brentner, "The Uses and Abuses of the Acoustic Analogy in Helicopter Rotor Noise Prediction," AHS Specialists; Meeting on Aerodynamics and Aeroacoustics, Arlington, Texas, February 25-27, 1987
15. Brentner, K.S., "Numerical Algorithms for Acoustic Integrals -- the Devil is in the Details," AIAA Paper No. 96-1706, 1996.
16. Lockard, D. P., "An Efficient, Two-Dimensional Implementation of the Ffowcs Williams and Hawkings Equation," *Journal of Sound and Vibration*, Vol 229, No. 4., pp. 897-911, 2000.
17. Girimaji, S., private communication, 2001.
18. Spalart, P., Jou, W.-H., Strelets, M., and Allmaras, S.R., "Comments on the Feasibility of LES for Wings, and on a Hybrid RANS/LES Approach," In *Advances in DNS/LES*, C. Liu & Z. Liu, Eds., Greyden Press, Columbus, OH, 1997.
19. Morris, P.J., Giridharan, M.G., and Lilley, G.M., "On the Turbulent Mixing of Compressible Free Shear Layers," Proc. Roy. Soc., London, Ser. A., Vol. 431, pp. 219-243, 1990.
20. Menter, F., "Improved Two-Equation k-ω Turbulence Models for Aerodynamic Flows," NASA TM 103975, 1992.
21. Khorrami, M. R., Singer, B. A., and Berkman, M. E., "Time-Accurate Simulations and Acoustic Analysis of Slat Free-Shear Layer," AIAA Paper 2001-2155, May 2001.
22. Khorrami, M.R., Berkman, M.E., and Choudhari, M., "Unsteady Flow Computations of a Slat with a Blunt Trailing Edge," AIAA J., Vol. 38, No. 11, 2000, pp. 2050-2058.
23. Singer, B.A., Lockard, D.P., and Brentner, K.S., "Computational Aeroacoustic Analysis of Slat Trailing-Edge Flow," AIAA J., Vol. 38, No. 9, 2000, pp. 1558-1564.
24. Khavran, A., Krejsa, E.A., and Kim,C.M., "Computation of Supersonic Jet Noise for an Axisymmetric Convergent-Divergent Nozzle," J. Aircraft, Vol. 31, May 1994, pp. 603-609.
25. Tam, C.K.W. and Auriault, L., "Jet Mixing Noise from Fine-Scale Turbulence," AIAA Paper 98-2354, 1998.
26. Manoha, E., Elias, G., Troff, B., Sagaut, P, "Towards the Use of Boundary Element Method in Computational Aeroacoustics," AIAA Paper 99-1980, 1999.
27. Atkins, H. L. and Shu, C. W., "Quadrature-Free Implementation of Discontinuous Galerkin Method for Hyperbolic Equations," AIAA Journal, Vol. 36, No. 5, 1997, pp. 775-782.

Table 1. C_L and C_D as function of angle-of-attack (AOA)

AOA (degrees)	C_L (unsteady)		C_D (unsteady)		C_L (steady)	C_D (steady)
	mean	r.m.s.	mean	r.m.s.		
4	2.607	0.0108	0.0766	0.0063	2.61	0.078
6	2.836	0.0094	0.0899	0.0058	(Not computed)	
8	3.069	0.0040	0.1028	0.0017	3.07	0.103

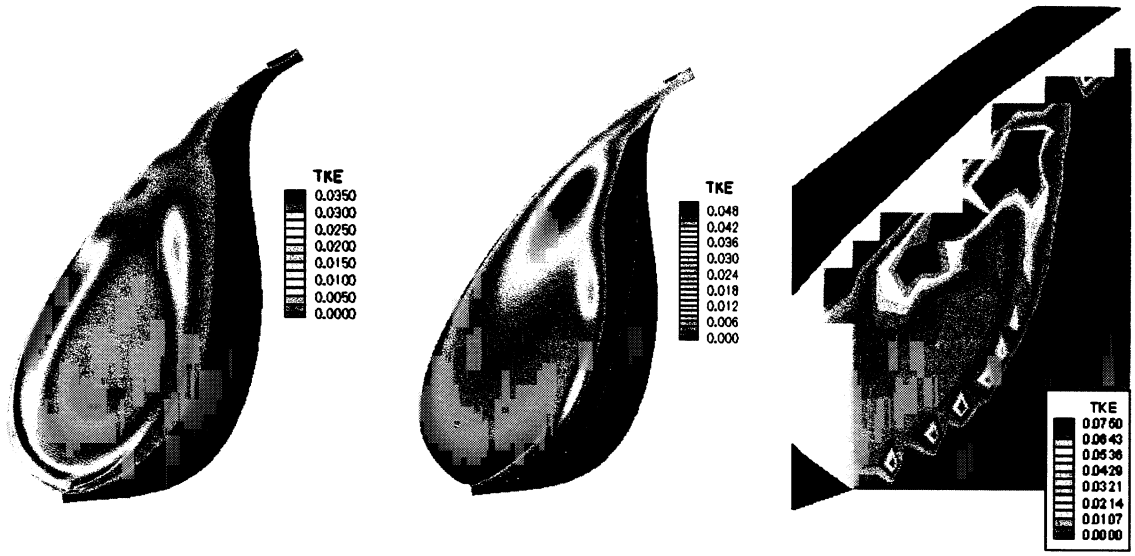

(a) URANS calculation with zonal model (b) Steady RANS calculation (c) PIV data from Ref. [2]

Figure 3. A comparison of turbulent kinetic energy based on unsteady and steady RANS calculations at 8 degree AOA, plus experimental measurements at 5 degree AOA.

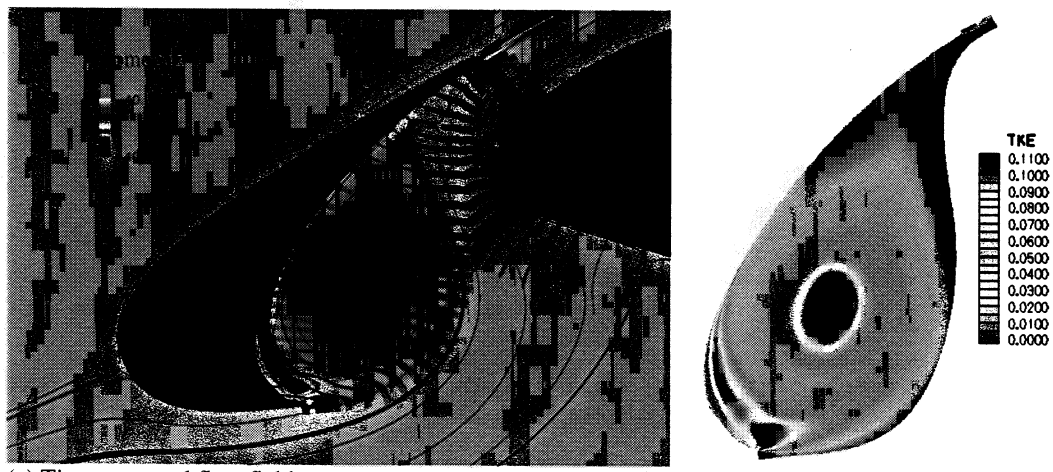

(a) Time averaged flow field (b) TKE distribution

Fig. 4. Unsteady RANS solution with zonal turbulence model at 4 degree AOA.

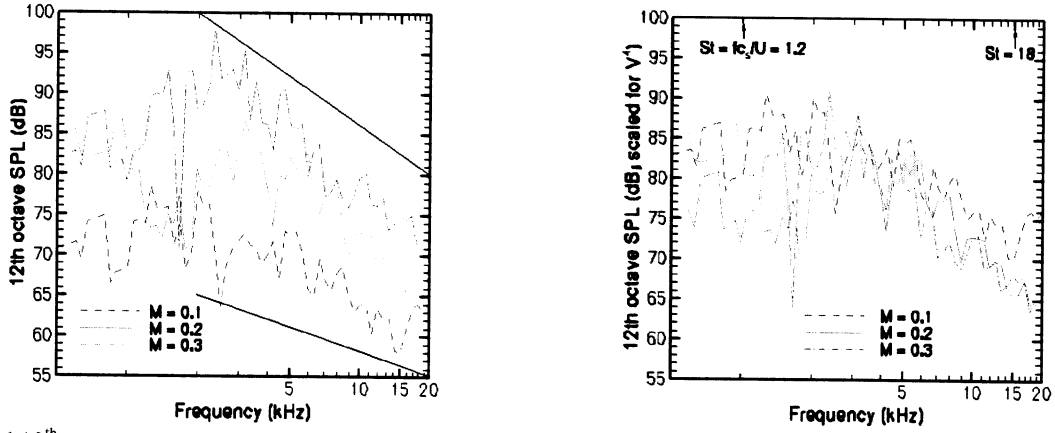

(a) Unscaled 12th octave SPLs (solid black lines indicate decay in 12th octave levels according to f^{-1} and f^{-2}, respectively).

(b) 12th octave SPLs scaled according to V^4 law

Fig. 8. Velocity scaling laws for computed noise levels at 8 deg AOA (M = 0.2, Re_L = 7.2 million). The Strouhal frequency is scaled with respect to slat chord c_s and free-stream speed U; result for M = 0.2 is based on ref. [1].

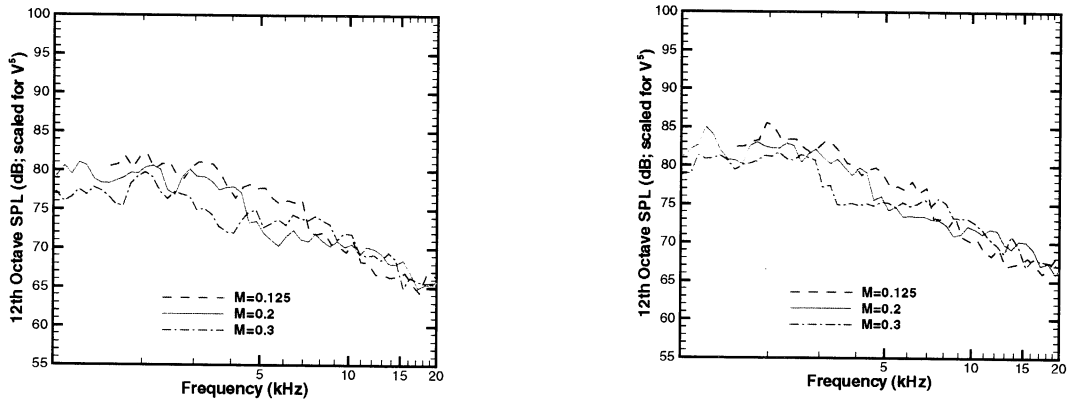

(a) AOA = 9 deg.

(b) AOA = 6 deg

Fig. 9. Velocity scaling for measured noise in LTPT experiment[3] for M = 0.2, Re_L = 7.2 million: 12th octave SPLs scaled according to V^5 law

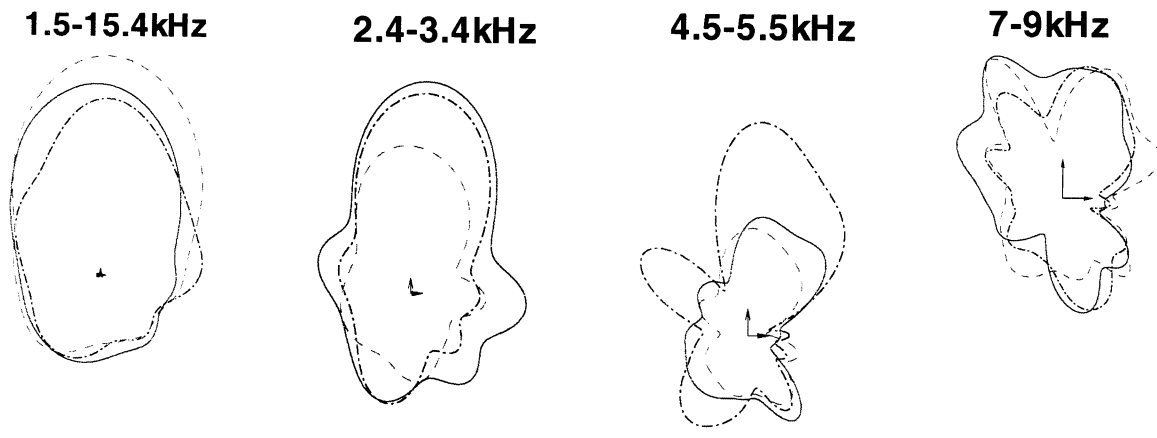

(a) (b) (c) (d)

Fig. 10. Broadband plus narrow-band directivity patterns for far-field noise computed with URANS+FWH (M=0.2, Re_L = 7.2 million, 4 degree AOA, 30 deg. slat and flap deflections)